Extremely Robust Pulse Retrieval From Even Noisy Second-Harmonic-Generation Frequency-Resolved Optical Gating Traces

Rana Jafari and Rick Trebino, *Member, IEEE*

***Abstract*— We further improve and then demonstrate the reliability of the previously introduced RANA approach for the second-harmonic-generation frequency-resolved optical gating (SHG FROG) phase-retrieval algorithm in the presence of significant noise in the traces. We provide a set of relevant parameters for this approach according to the noise level and trace size. Using it, we achieve 100% convergence for thousands of even extremely complex sample pulses, even when contaminated with the introduced significant noise.**

***Index Terms*— Optical pulses, phase retrieval, pulse measurements, ultrafast optics.**

I. Introduction

THE frequency-resolved-optical-gating (FROG) technique measures the complete temporal electric field vs. time of arbitrary ultrashort laser pulses without the need for assumptions or reference pulse [1]. It has been highly developed and optimized, has many applications, and is an increasingly standard technique for measuring ultrashort laser pulses over a wide range of wavelengths, pulse lengths, and complexities. It operates by acquiring spectra of optical signal fields generated from the nonlinear-optical interaction between variably delayed replicas of the pulse in a medium. This yields a two-dimensional data trace $I_{FROG}(\omega, \tau)$ of intensity as a function of angular frequency ω and the relative delay τ between the replica pulses.

Direct retrieval of the pulse field from a measured FROG trace is not possible, so indirect, iterative algorithms have been developed over the years to retrieve the pulse from its measured trace. Early efforts were unreliable and/or overly complex [2], [3]. The generalized-projections approach [4], however, was a significant step forward, achieving much higher reliability with relatively straightforward implementation. Its reliability (convergence probability) is ∼90% for relatively simple pulses. But this probability falls to ∼50% as the pulse complexity increases from simple-pulse time-bandwidth products (TBPs) of ∼1 to complex-pulse TBPs of ∼100 (and depending on the noise present and the particular version of FROG) [5], [6]. Other FROG algorithms have been introduced, but they either address different issues, such as missing data or programming ease [7] and not reliability. Ideally, convergence would occur 100% of the time even when the measured trace is very noisy. So, we address this issue and solve this problem here.

Manuscript received September 19, 2019; revised October 23, 2019; accepted October 25, 2019. Date of publication October 30, 2019; date of current version December 9, 2019. This work was supported in part by the National Science Foundation under Grant ECCS-1609808 and in part by the Georgia Research Alliance. *(Corresponding author: Rana Jafari.)*

The authors are with the School of Physics, Georgia Institute of Technology, Atlanta, GA 30332 USA (e-mail: rjafari7@gatech.edu; rick.trebino@physics.gatech.edu).

Color versions of one or more of the figures in this article are available online at http://ieeexplore.ieee.org.

Digital Object Identifier 10.1109/JQE.2019.2950458

II. SHG FROG and Its Algorithm

Second-harmonic generation (SHG) is the most commonly used nonlinearity for FROG's experimental setup due to its sensitivity and simple geometry. Mathematically, the SHG FROG trace is given by [1]:

$$I_{FROG}^{SHG}(\omega, \tau) = \left| \int_{-\infty}^{\infty} E_{sig}(t, \tau) \exp(-i\omega t)\, dt \right|^2 \tag{1a}$$

where:

$$E_{sig}(t, \tau) = E(t)E(t - \tau) \tag{1b}$$

The SHG FROG iterative phase-retrieval algorithm reconstructs the unknown complex field, $E(t)$, by finding the signal field $E_{sig}(t,\tau)$ from the measured FROG trace using the above two equations, that is, these two constraints. Specifically, it first uses the measured data in the frequency and delay domains, which, as shown in Eq. (1a), is the squared magnitude of the Fourier transform of the signal field. Second, it uses the mathematical relation for the signal field in the time and delay domains, which, for SHG FROG, is given by Eq. (1b).

The goal of the algorithm is to find the temporal complex electric field of a pulse, $E(t)$, which can be written as the complex-field amplitude in the time or, equivalently, frequency domain:

$$E(t) = \sqrt{I(t)} \exp\left(-i\phi(t)\right), \tag{2a}$$

$$\tilde{E}(\omega) = \sqrt{S(\omega)} \exp\left(-i\varphi(\omega)\right), \tag{2b}$$

where $I(t) = |E(t)|^2$ is the pulse intensity and $\phi(t)$ is the phase, both as a function of time, t, respectively. Also, $S(\omega)$ is the pulse spectrum and $\varphi(\omega)$ is the spectral phase, both as a function of frequency ω. Knowledge of the complex field vs. either time or frequency yields the complete pulse.

0018-9197 © 2019 IEEE. Personal use is permitted, but republication/redistribution requires IEEE permission.
See http://www.ieee.org/publications_standards/publications/rights/index.html for more information.

Authorized licensed use limited to: Georgia Institute of Technology. Downloaded on December 09,2020 at 18:47:12 UTC from IEEE Xplore. Restrictions apply.

An excellent and unusual feature of all versions of FROG is that they also provide feedback on the quality of the measurement. There is a unique relation between the field and its FROG trace [8], [9]. Also, the trace, an $N \times N$ array, has N^2 points, far more points than the pulse, which has only N intensity points and N phase points, where typically, $N \sim 100$ or more. Thus, when agreement occurs between the measured trace and the trace reconstructed from the retrieved pulse, one can conclude with a high degree of certainty that the pulse was correctly measured.

On the other hand, if FROG is used to measure an unstable pulse train, the trace will be the sum of many different FROG traces (essentially one for each pulse in the train), and there is no single field whose trace corresponds to the measured trace. Therefore, the FROG algorithm, which can only return a single pulse, cannot return a perfectly meaningful result. Simulations have shown that, fortunately, it returns a pulse fairly close to the typical field of the pulses in the train. In the presence of such instability, however, the retrieved FROG *trace* corresponding to the retrieved field cannot agree with the measured one [10]–[12], tipping off the user to the presence of instability. More recently, algorithms have been developed to extract additional information from FROG traces corresponding to such partially coherent pulses [13], [14]. In general, the rule of thumb resulting from this work is that disagreement between the measured and retrieved traces is the key indicator of pulse-shape instability.

Unfortunately, there is another instance when this disagreement might occur, and that is when the pulse-retrieval algorithm does not converge to the correct solution, that is, it *stagnates*. Hence, additional attempts for the recovery of the field using the algorithm are typically needed [6]. But there is always the chance that the algorithm will stagnate as many times as the user is willing to run it, thus making it difficult to distinguish between the two very different cases of algorithm stagnation and pulse-train instability.

III. The RANA Approach

Consequently, a highly reliable FROG algorithm is critically required in order to avoid this uncertainty. Fortunately, one has recently been introduced. It is called the Retrieved-Amplitude N-grid Algorithmic (RANA) approach, and variations of it work for SHG FROG [15] and also other versions of FROG, including the polarization-gate (PG) and transient grating (TG) FROG techniques [16]. For all of these FROG variations, it yielded 100% convergence even when tested on very large samples of pulses (over 20,000) and even with extremely high complexity—TBPs as high as 100—and large array sizes and in the presence of noise in the traces [15], [16].

The RANA approach first involves retrieving the spectrum of the pulse *directly* from the trace. For SHG FROG, it does this using the trace "frequency marginal," which is obtained by integrating the trace over the delay variable, and, in SHG FROG, it can be shown to be equal to the autoconvolution of the spectrum, $S(\omega)$ [1]:

$$M^{SHG}(\omega) = \int_{-\infty}^{+\infty} I^{SHG}_{FROG}(\omega, \tau)\, d\tau = S(\omega) * S(\omega). \qquad (3)$$

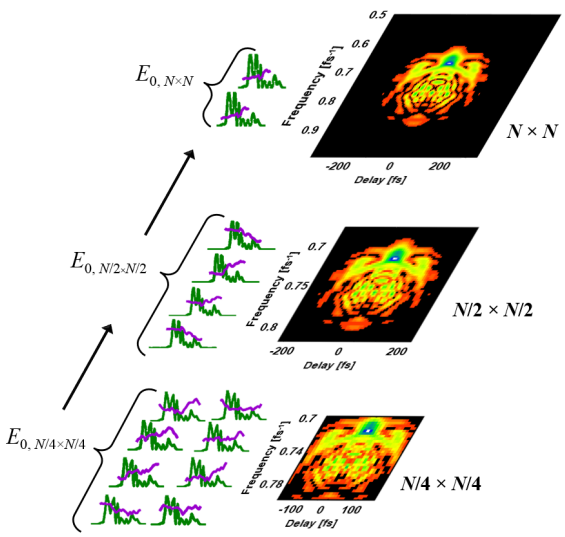

Fig. 1. Schematic representation of the multi-grid component of the RANA approach. E_0 corresponds to the set of the initial guesses.

This result has recently been shown to be invertible to directly yield the spectrum [15]. Next, we generate a set of about a dozen initial guesses, all with the above-derived spectrum and each with a different, random spectral phase. These pulses are then used in iterations on smaller and coarser trace grids, in what is called a "multi-grid" scheme [17], [18], and only the few best pulses are kept. Lastly, these few best pulses are provided to the full FROG trace for a few final iterations to completely determine the pulse. See Fig. 1. This approach proved *perfectly* reliable, with no stagnations for over 25,000 traces pulses in the presence of small amounts of noise [15]. Even better, it also proved faster for more complex pulses. And a variation on it performed equally well for other common FROG beam geometries [16].

As the FROG trace becomes contaminated with more noise, however, the frequency-marginal curve begins to deviate more from the exact autoconvolution of the spectrum, and hence the direct retrieval of the spectrum becomes proportionally less accurate and also more challenging. In the initial implementation of the RANA approach for SHG FROG [15], we simply considered its viability, so the analysis was performed with only small amounts (0.5%) of multiplicative noise added to the SHG FROG traces. In view of the possibility that additional noise in the trace could defeat this approach, it is important to consider traces with more noise. So, in this work, we test the RANA approach and, in particular, the performance of the direct retrieval of the spectrum from the frequency marginal of SHG FROG in the presence of considerable amounts of both multiplicative and additive measurement noise. We introduce a few additional simple tricks to the approach that were not used in our earlier work, as they had proven unnecessary then, but here, in the presence of significant noise, we find that they are, in fact, useful. Finally, we provide a procedure for determining the number of required initial guesses and iterations used in the multi-grid component of the approach based on the amount of noise in the given trace such that a 100% reliable retrieval from such traces is still achieved for thousands of test pulses.

Authorized licensed use limited to: Georgia Institute of Technology. Downloaded on December 09,2020 at 18:47:12 UTC from IEEE Xplore. Restrictions apply.

IV. Direct Retrieval of the Spectrum From Noisy Traces

To obtain the spectrum directly from the frequency marginal of the trace, we use the convolution theorem, which yields:

$$s_{\pm}(t) = \pm\sqrt{\mathscr{F}^{-1}\{S(\omega) * S(\omega)\}}, \tag{4}$$

where $s(t)$ is the inverse Fourier transform of $S(\omega)$. Taking the square root yields $s(t)$, but with ambiguity in the sign of the roots, so we define $s_{\pm}(t)$, according to whether the real part of $s_{\pm}(t)$ is positive or negative. This ambiguity is removed by taking advantage of the Paley-Wiener theorem [19], which states that the inverse-Fourier transform of a band-limited signal (here, the spectrum) is infinitely differentiable. We apply this smoothness criterion to $s_{\pm}(t)$ using a weighted sum of zeroth- to second-order derivatives [15].

Specifically, we have used the following weighted sum as the criterion for determining the sign:

$$\varepsilon_{\pm} \equiv \alpha\ |\Delta_{0\pm}|^2 + \beta\ |\Delta_{1\pm}|^2 + \gamma\ |\Delta_{2\pm}|^2, \tag{5}$$

where $\alpha = 0.09, \beta = 0.425, \gamma = 1$ are the previously determined weights in [15]. Also, these differences are given below, where $s(t_{k<i+1})$ refers to a value of $s(t)$ for which a sign has already been assigned:

$$\begin{aligned} \Delta_{0\pm} &= s_{\pm}(t_{i+1}) - s(t_i), \\ \Delta_{1\pm} &= \left[s_{\pm}(t_{i+1}) - s(t_i)\right] - \left[s(t_i) - s(t_{i-1})\right], \\ \text{and,}\quad \Delta_{2\pm} &= \left\{\left[s_{\pm}(t_{i+1}) - s(t_i)\right] - \left[s(t_i) - s(t_{i-1})\right]\right\} \\ &\quad - \left\{\left[s(t_i) - s(t_{i-1})\right] - \left[s(t_{i-1}) - s(t_{i-2})\right]\right\}. \end{aligned}$$

The root corresponding to the smaller ε is selected for each temporal point.

Fig. 2 shows this process for a typical pulse. Note that simple continuity of $s(t)$ ($\Delta_{0\pm}$) is sufficient to determine the correct root for the overwhelming majority of values of t. But, when both real and imaginary values of s are close to zero, continuity of the first derivative becomes the deciding factor. We also include the second derivative just in case it helps. Of course, infinitely many additional derivatives could also be used, but noise is likely to render them unhelpful.

However, as mentioned, as the trace becomes corrupted with more noise, the frequency marginal deviates from the exact curve corresponding to the autoconvolution of the spectrum (see Fig. 3). Specifically, we find that the original approach we discussed in [15] then does not retrieve the correct spectrum on occasion. For example, for the highly challenging case of extremely complex pulses with TBPs of ~40 with massive noise (5% multiplicative and 3% additive) in the trace, it is only successful in achieving the correct spectrum (that is, with an rms error of less than 9%) 30% of the time. We should emphasize here that, while it is not essential that the above deconvolution process retrieve the precise spectrum, *as it is only used as an initial guess for the usual FROG algorithm*, which performs fairly well even with random noise as an initial guess, it is preferable to optimize it for cases of very high noise. Indeed, it is, of course, best to retrieve the spectrum as well as possible. Fortunately, there were additional constraints that we did not take advantage of in that work, and which we do here.

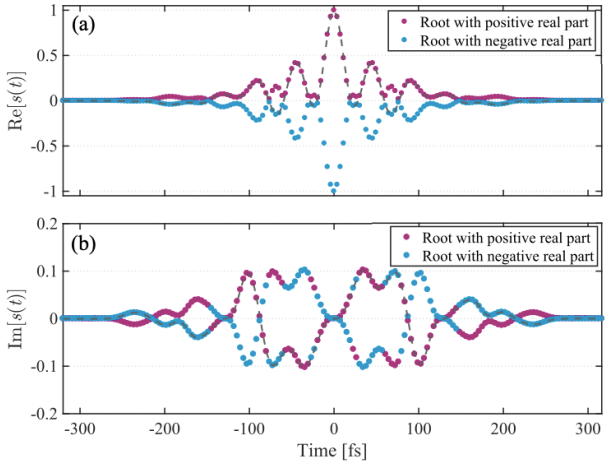

Fig. 2. Plots of real (a) and imaginary (b) parts of $s_{\pm}(t) = \pm\sqrt{\mathscr{F}^{-1}\{M^{SHG}(\omega)\}}$. The roots with positive real parts are shown in purple, and the roots with negative real parts are shown in blue. The correct signs of the roots are easily obtained by applying the continuity and derivative-continuity conditions on the real and imaginary parts of the root and are shown by the dashed gray line.

Therefore, in this work, we include additional approaches to enhance the performance of the RANA approach. Specifically, we determine the temporal points at which both the real and imaginary parts of $s(t)$ are close to zero (where decisions are the most difficult and hence most likely to go awry due to noise), and the alternative signs of the roots after these points are also used for determining the spectrum of the pulse (see Fig. 4).

In addition, because the spectrum is always real, the real part of its inverse-Fourier transform, $s(t)$, must be even, and the imaginary part odd. Thus, we need only determine the left half (negative times) or right half (positive times) of the $s(t)$ curve; the other is then determined by the above symmetry condition. So, we consider only the left half of the time values and then only the right half, yielding two, possibly somewhat different, curves for $s(t)$.

The combination of applying the weighted sums and also using alternative signs after the roots that are close to zero leads to a set of curves obtained from the left and right sides of $s_{\pm}(t)$. Next, the resulting autoconvolutions of these curves are obtained and compared with the frequency marginal of the trace.

Another constraint that we now take advantage of is the fact that the spectrum must also be positive definite. So we select the spectrum whose autoconvolution yields the smallest rms difference with the frequency marginal. We also kept no more than 25 of the extra generated spectra based on their closeness to the frequency marginal and their positivity (this value would be smaller depending on the number of extra generated curves). Next, three additional spectra used for the initial guesses are selected from this remaining set of less than 25 spectra with the caveat that they are fairly different from the previously selected spectra (based on the rms differences from each of the previously selected curves for the spectra).

Authorized licensed use limited to: Georgia Institute of Technology. Downloaded on December 09,2020 at 18:47:12 UTC from IEEE Xplore. Restrictions apply.

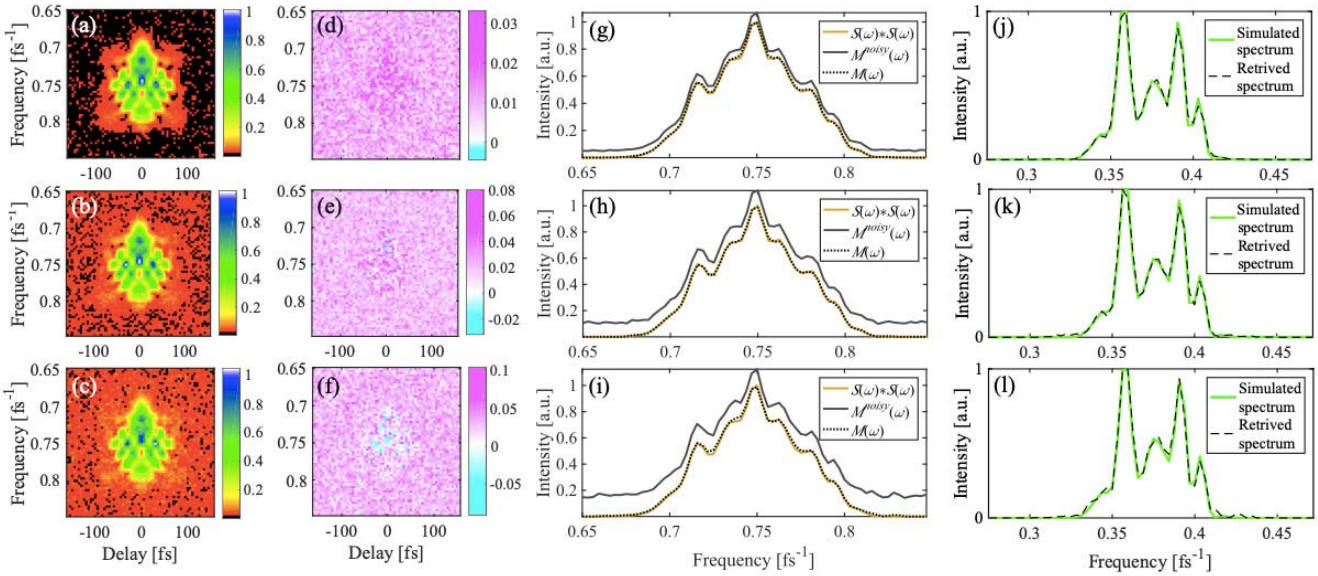

Fig. 3. (a-c) Noisy SHG FROG traces with multiplicative noise of 1%, 3%, and 5% and additive noise of 1%, 2%, and 3%, respectively. (d-f) The difference between the noisy trace and the noiseless simulated traces. (g-i) The autoconvolution of the spectrum (orange), marginal obtained from noisy trace $M^{noisy}(\omega)$ (gray), and marginal after noise suppression (dotted black), $M(\omega)$. (j-l) The simulated and retrieved spectra obtained directly from the frequency marginal, $M(\omega)$.

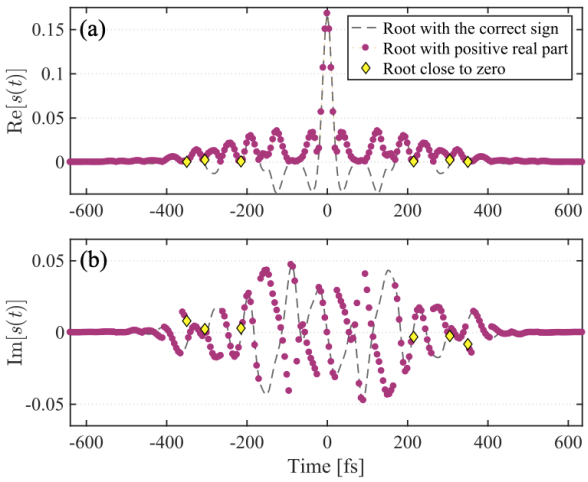

Fig. 4. Example of points where the sign decisions are the most likely to be wrong. (a) Real and (b) imaginary parts of roots corresponding to the root with positive real part, $s_+(t)$, for a complex pulse shown with purple circles. The points where both real and imaginary parts are close to zero are shown with yellow markers. At these points, alternative signs of roots are taken into consideration. The correct curves for the real and imaginary parts of $s(t)$ are indicated by the dashed gray line.

It is also worth mentioning that, as is generally done, low-pass filtering is first performed on the measured trace [5]. In addition, we apply background subtraction, but on the marginal curve, $M^{SHG}(\omega)$, rather than the entire trace, for the purpose of retrieving the spectrum.

Additionally, we use $\mathscr{F}^{-1}\{M^{SHG}(\omega)\}$ in its original length, N, without zero-padding to the length $2N$, as was done in [15], as we found zero-padding to be unnecessary.

V. Results

We tested the robustness of the RANA approach on sets of pulses with rms time-bandwidth products ($TBP = \tau_{rms}\omega_{rms}$) of 2.5, 10, and 40, with array sizes of 64×64, 256×256, and 1024×1024, respectively (where 0.5 is the TBP of a Fourier-transform-limited Gaussian pulse). We estimated the required parameters of the RANA approach for three levels of noise, and they are given in Table I. These parameters include the number of initial guesses and iterations on each grid, based on the pulse complexity and noise in the trace.

Fig. 5 shows an instance where consideration of an alternative sign of the root at one of the points of $s(t)$ that is close to zero was effective in determining the correct spectrum.

The performance of the direct spectral retrieval from the frequency marginal of the set of pulses with $TBP = 10$ contaminated with 3% multiplicative and 2% additive noise is shown in Fig. 6 where the distribution of rms differences between the simulated spectrum and four selected spectra are given, as well as the lowest rms difference among all four chosen spectra as the initial guesses.

Fig. 7 provides representative retrieval results for a set of pulses with $TBP = 10$ in the presence of significant noise (5% multiplicative and 3% additive noise).

For the set with $TBP = 2.5$, the direct spectral retrieval step was successful (that is, the rms difference between the actual and retrieved spectra less than 9%) for more than 99.5% of cases. This rate is 99.8% to 96.5% and 95% to 77% for sets with $TBP = 10$ and 40, respectively, as the noise increases over the values considered here. However, we emphasize again that it should be kept in mind that these spectra are only used as *initial guesses*, rather than the final results, so these success rates are excellent. Indeed, prior to the RANA approach, initial guesses of random noise or simple fixed-width Gaussians were

Authorized licensed use limited to: Georgia Institute of Technology. Downloaded on December 09,2020 at 18:47:12 UTC from IEEE Xplore. Restrictions apply.

TABLE I

(A) PARAMETERS USED FOR PULSES WITH $TBP = 2.5$, AND ARRAY SIZE 64×64 (IG: INITIAL GUESS). (B) PARAMETERS USED FOR PULSES WITH $TBP = 10$, AND ARRAY SIZE 256×256 (IG: INITIAL GUESS). (C) PARAMETERS USED FOR PULSES WITH $TBP = 40$, AND ARRAY SIZE 1024×1024 (IG: INITIAL GUESS)

(A)

Multiplicative Noise	Additive Noise	# of IGs $N/4\times N/4$ array	# of iterations $N/4\times N/4$ array	# of IGs $N/2\times N/2$ array	# of iterations $N/2\times N/2$ array	# of IGs $N\times N$ array	G/G' error $N\times N$ array
1%	1%	16	20	8	15	4	0.007 / 0.08
3%	2%	16	25	12	25	4	0.008 / 0.10
5%	3%	20	30	12	25	4	0.009 / 0.12

(B)

Multiplicative Noise	Additive Noise	# of IGs $N/4\times N/4$ array	# of iterations $N/4\times N/4$ array	# of IGs $N/2\times N/2$ array	# of iterations $N/2\times N/2$ array	# of IGs $N\times N$ array	G/G' error $N\times N$ array
1%	1%	24	20	12	15	4	0.004 / 0.08
3%	2%	32	30	16	30	4	0.006 / 0.10
5%	3%	36	35	20	30	4	0.0075 / 0.12

(C)

Multiplicative Noise	Additive Noise	# of IGs $N/4\times N/4$ array	# of iterations $N/4\times N/4$ array	# of IGs $N/2\times N/2$ array	# of iterations $N/2\times N/2$ array	# of IGs $N\times N$ array	G/G' error $N\times N$ array
1%	1%	32	30	20	25	4	0.0035 / 0.08
3%	2%	36	30	24	30	4	0.0055 / 0.10
5%	3%	40	35	24	30	4	0.007 / 0.12

TABLE II

NUMBER OF SAMPLE PULSES AND AVERAGE RETRIEVAL TIMES FOR THE SAMPLE SET OF PULSES IN THE THREE NOISE LEVELS

Multiplicative Noise	Additive Noise	$TBP = 2.5$		$TBP = 10$		$TBP = 40$	
		Average retrieval time	Number of pulses	Average retrieval time	Number of pulses	Average retrieval time	Number of pulses
1%	1%	0.15s	5000	1.1s	5000	35s	1000
3%	2%	0.20s	5000	2.1s	5000	45s	1000
5%	3%	0.24s	5000	2.6s	5000	49s	1000

used as initial guesses, and convergence rates of >50% were achieved, despite such inaccurate initial guesses.

We considered a pulse retrieval to have converged to the correct solution when the G error (the rms difference between the measured and retrieved traces) or G' error (the trace-intensity-weighted rms difference between the measured and retrieved traces) were reached to either of the cutoff values given in Table I. These values appropriately depend on the trace size and amount of noise. As the traces become smaller and noisier, the expected G error increases. However, the G' convergence criterion depends only on the noise value and is independent of the trace dimension. In the presence of significant noise, in addition to the visual agreement between the measured and retrieved traces, the G' error is a generally better measure of the success of the retrieval but, its use is not essential to the process.

For the multi-grid step, in moving from one grid to the next, the best retrieved results based on the value of G (or G') error are selected. Next, each of the four directly retrieved spectra is replaced with the one retrieved after some iterations by the usual generalized-projections (GP) phase retrieval algorithm for FROG [1] or any other FROG algorithm the user prefers, and the G (or G') errors of the resulting traces are compared. If the process yields a smaller G (or G') error, the spectrum is replaced with the best one at this point. Even though this step might increase the overall retrieval time, as four additional traces for each of the initial guesses are obtained and the resulting G errors are calculated, it leads to a better initial guess. Table II presents the average retrieval times using the same computer and programing language (MATLAB) as in our previous work.

We found that the RANA approach converged to the correct pulse for every pulse in our sample of 15,000 pulses.

Because the RANA process worked so well, instead of plotting "typical" results, we plot our absolute *worst* results in Figs. 8 and 9, corresponding to the largest G error for the given pulse sets, with $TBP = 2.5$ and 40, respectively, each corrupted with 5% multiplicative and 3% additive noise. Note the excellent agreement between actual and retrieved pulses in both cases.

VI. DISCUSSION AND CONCLUSION

Overall, we have found that the original implementation of the RANA approach works quite well, even in the presence

Authorized licensed use limited to: Georgia Institute of Technology. Downloaded on December 09,2020 at 18:47:12 UTC from IEEE Xplore. Restrictions apply.

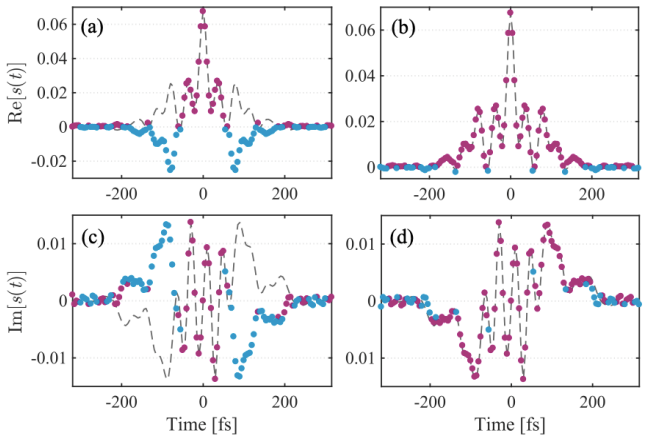

Fig. 5. The circles (purple/blue: root with the positive/negative real part) show the real (a, b) and imaginary (c, d) parts of the root corresponding to the curves obtained by applying the weighted sum for smoothening the roots (a, c), and the curve when the alternative sign of root is considered after a point where both the real and imaginary parts of root are close to zero (b, d). The correct curves for real and imaginary parts of $s(t)$ are shown by the dashed gray line. It can be seen from (b) and (d) that considering the alternative signs of root after a root close to zero yields the correct spectrum.

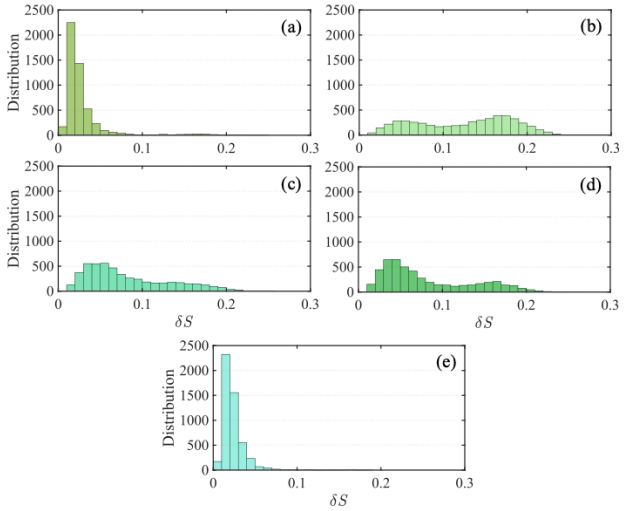

Fig. 6. Distribution of rms errors, δS, between the simulated spectra and four retrieved spectra for 5000 pulses from frequency marginals of SHG traces contaminated with 3% of multiplicative noise and 2% of additive noise (a-d). (a) Corresponds to the spectrum with an autoconvolution yielding the smallest rms difference from the marginal, while those in (b) through (d) are alternative spectra obtained by using alternative (less likely) roots, as described in the text. (e) Distribution of the minimum value of rms error among the four spectra for each pulse. Note that the first choice for the spectrum is nearly always the best, but the others could be helpful in cases of considerable noise.

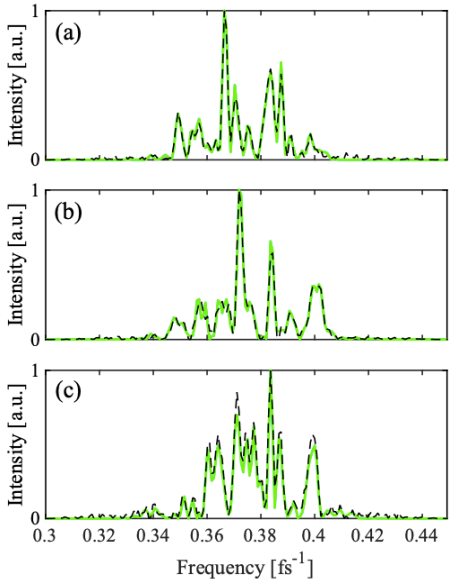

Fig. 7. Direct spectral retrieval results from SHG traces, with $TBP = 10$, contaminated with 5% multiplicative and 3% additive noise. (a) Retrieved spectra in the top 25%, (b) the middle 50%, and (c) the bottom 25% of the rms difference distributions. The simulated spectrum is given in light green line, and the best-retrieved spectra are shown by dashed black lines. All of the results show good agreement with the simulated spectra. Indeed, as the retrieved spectra are only used as initial guesses, these results are more than sufficient for pulse retrieval.

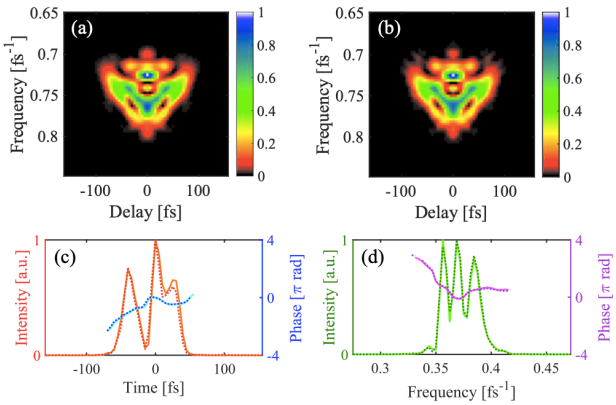

Fig. 8. Worst-case pulse-retrieval result for a pulse with $TBP = 2.5$ for a trace with 5% multiplicative and 3% additive noise. $G' = 0.0854 < G'_{cut-off}$, and $G = 0.0102$. (a) Simulated FROG trace before applying the noise. (b) Retrieved FROG trace. (c, d) Simulated and retrieved temporal/spectral field (orange/green: simulated temporal/spectral intensity; cyan/magenta: simulated temporal/spectral phase; red/dark green: retrieved temporal/spectral intensity; blue/purple: retrieved temporal/spectral phase).

of significant multiplicative and additive noise. However, we found that improving it slightly allows it to work even better—indeed, extremely well even in the presence of significant noise. In summary, our improved RANA approach (including standard techniques) involves these steps:

1. Fourier-filter the measured trace.
2. Compute the trace frequency marginal.
3. Subtract any background from the frequency marginal.
4. Inverse-Fourier-transform the frequency marginal and compute the two square roots (+/−) of it for all times.
5. For negative times, start on the left (the most negative time), and choose the root that minimizes the sum of the derivative differences.
6. Find the local minima of the real part of the positive root and keep points for which both the real and imaginary parts are close to zero. Retain the alternative signs of the roots after these points.
7. For positive times, use +/− the mirror image of $s(t)$ for negative times in order to obey the reality condition for the spectrum.

Authorized licensed use limited to: Georgia Institute of Technology. Downloaded on December 09,2020 at 18:47:12 UTC from IEEE Xplore. Restrictions apply.

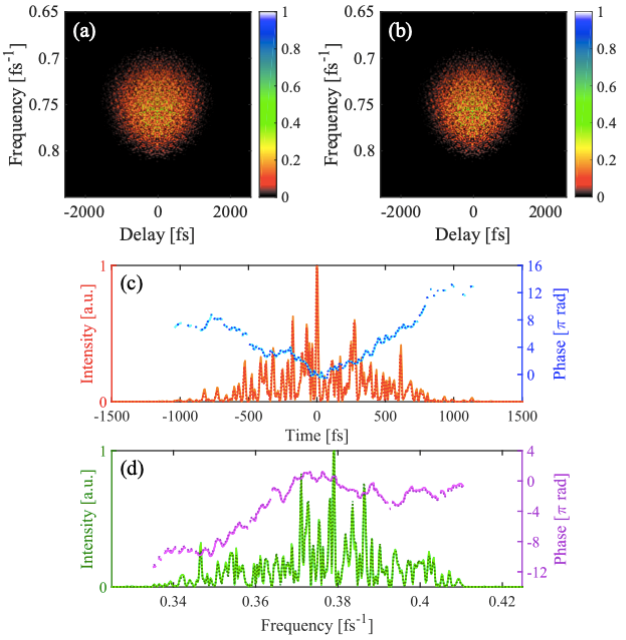

Fig. 9. Worst-case pulse-retrieval result for a pulse with $TBP = 40$ for a trace with 5% multiplicative and 3% additive noise. $G = 0.0065 < G_{cut-off}$ and $G' = 0.1506$. (a) Simulated FROG trace before applying the noise. (b) Retrieved FROG trace. (c, d) Simulated and retrieved temporal/spectral field (orange/green: simulated temporal/spectral intensity; cyan/magenta: simulated temporal/spectral phase; red/dark green: retrieved temporal/spectral intensity; blue/purple: retrieved temporal/spectral phase).

8. For positive times, repeat steps 5-7, but beginning at $t = 0$, and proceeding rightward to increasingly positive times.
9. Keep only the four best solutions for $s(t)$, comparing their autoconvolution with the frequency marginal, their positivity, and uniqueness to evaluate them (see the text for details, although the details of the approach used here are not important).
10. Generate a number (see Table I) of initial guesses using the above retrieved spectra and random spectral phases.
11. Run the GP algorithm (or any other FROG algorithm) on these initial guesses for a number of iterations (see Table I) using the $N/4 \times N/4$ array.
12. Keep only the best pulses (see Table I) and run the FROG algorithm on them for the $N/2 \times N/2$ array, again keeping only the best pulses when this is complete.
13. Run the remaining four best pulses for the complete FROG trace, choosing the result with the lowest G or G' error as the solution.

The above approach achieves convergence for all pulses that we tried, even in the presence of massive noise. While the changes we made here were mostly minor, including additional roots of the inverse-Fourier transform of the spectrum appears to add the most to its reliability—enough to handle rather large amounts of noise in the traces. With the use of this slightly modified RANA approach, we achieved 100% convergence on three sets of pulses with even very high complexities and contaminated with low to quite high levels of noise that are more likely to be present in experimental FROG traces of stable pulse trains. We believe that SHG FROG's pulse-retrieval algorithm is now effectively foolproof for the very general type of measurement noise considered here. In this work, we have used the usual GP algorithm [1] in the RANA approach, but this algorithm could simply be replaced by any other FROG pulse-retrieval algorithm.

For the full trace, we use only four pulses, but convergence almost always occurs on the first one.

Except for a very slight increase in convergence time for very simple pulses, we find that there is essentially no "downside" to the RANA approach, as, for more complex pulses, it is even faster than the FROG algorithm upon which it is based. Of course, RANA lends itself naturally to parallel processing and so could operate even faster.

As FROG is currently the most popular complete pulse-measurement technique in the numerous fields that use ultrashort laser pulses, we believe that this work will result in significantly better measurements of, especially, shaped pulses in numerous fields. Also, arguably more importantly, any discrepancies between measured and retrieved traces can now be *attributed unambiguously to pulse-shape instability*. Finally, we believe that this improvement will help to convert more users from obsolete methods, such as autocorrelation, to more informative and reliable pulse measurements.

ACKNOWLEDGMENT

R. Trebino owns a company that sells pulse-measurement devices.

REFERENCES

[1] R. Trebino, *Frequency-Resolved Optical Gating: The Measurement of Ultrashort Laser Pulses*, Boston, MA, USA: Kluwer Academic, 2002.
[2] K. W. DeLong and R. Trebino, "Improved ultrashort pulse-retrieval algorithm for frequency-resolved optical gating," *J. Opt. Soc. Amer. A*, vol. 11, no. 9, pp. 2429–2437, 1994.
[3] R. Trebino and D. J. Kane, "Using phase retrieval to measure the intensity and phase of ultrashort pulses: Frequency-resolved optical gating," *J. Opt. Soc. Amer. A*, vol. 10, no. 5, pp. 1101–1111, 1993.
[4] K. W. DeLong, D. N. Fittinghoff, R. Trebino, B. Kohler, and K. Wilson, "Pulse retrieval in frequency-resolved optical gating based on the method of generalized projections," *Opt. Lett.*, vol. 19, no. 24, pp. 2152–2154, 1994.
[5] D. N. Fittinghoff, K. W. DeLong, R. Trebino, and C. L. Ladera, "Noise sensitivity in frequency-resolved optical-gating measurements of ultrashort pulses," *J. Opt. Soc. Amer. B*, vol. 12, no. 10, pp. 1955–1967, 1995.
[6] L. Xu, E. Zeek, and R. Trebino, "Simulations of frequency-resolved optical gating for measuring very complex pulses," *J. Opt. Soc. Amer. B*, vol. 25, no. 6, pp. A70–A80, 2008.
[7] P. Sidorenko, O. Lahav, Z. Avnat, and O. Cohen, "Ptychographic reconstruction algorithm for frequency-resolved optical gating: Super-resolution and supreme robustness," *Optica*, vol. 3, no. 12, pp. 1320–1330, 2016.
[8] D. J. Kane and R. Trebino, "Characterization of arbitrary femtosecond pulses using frequency-resolved optical gating," *IEEE J. Quantum Electron.*, vol. 29, no. 2, pp. 571–579, Feb. 1993.
[9] T. Bendory, P. Sidorenko, and Y. C. Eldar, "On the uniqueness of FROG methods," *IEEE Signal Process. Lett.*, vol. 24, no. 5, pp. 722–726, May 2017.
[10] J. Ratner, G. Steinmeyer, T. C. Wong, R. Bartels, and R. Trebino, "Coherent artifact in modern pulse measurements," *Opt. Lett.*, vol. 37, no. 14, pp. 2874–2876, 2012.
[11] R. Jafari and R. Trebino, "Pulse-chirp instability and issues for its measurement," in *Proc. Conf. Lasers Electro-Opt.*, 2018, Paper. JTh2A.142.
[12] M. Rhodes, Z. Guang, and R. Trebino, "Unstable and multiple pulsing can be invisible to ultrashort pulse measurement techniques," *App. Sci.*, vol. 7, no. 1, p. 40, 2017.

Authorized licensed use limited to: Georgia Institute of Technology. Downloaded on December 09,2020 at 18:47:12 UTC from IEEE Xplore. Restrictions apply.

[13] C. Bourassin-Bouchet and M. E. Couprie, "Partially coherent ultrafast spectrography," *Nature Commun.*, vol. 6, p. 6465, Mar. 2015.
[14] E. Escoto, R. Jafari, R. Trebino, and G. Steinmeyer, "Retrieving the coherent artifact in frequency-resolved optical gating," *Opt. Lett.*, vol. 44, no. 12, pp. 3142–3145, 2019.
[15] R. Jafari, T. Jones, and R. Trebino, "100% reliable algorithm for second-harmonic-generation frequency-resolved optical gating," *Opt. Exp.*, vol. 27, no. 3, pp. 2112–2124, 2019.
[16] R. Jafari and R. Trebino, "Highly reliable frequency-resolved optical gating pulse-retrieval algorithmic approach," *IEEE J. Quantum Electron.*, vol. 55, no. 4, Aug. 2019, Art. no. 8600107.
[17] C. W. Siders, J. L. W. Siders, F. G. Omenetto, and A. J. Taylor, "Multipulse interferometric frequency-resolved optical gating," *IEEE J. Quantum Electron.*, vol. 35, no. 4, pp. 432–440, Apr. 1999.
[18] R. Jafari and R. Trebino, "High-speed 'multi-grid' pulse-retrieval algorithm for frequency-resolved optical gating," *Opt. Exp.*, vol. 26, no. 3, pp. 2643–2649, 2018.
[19] R. S. Strichartz, *A Guide to Distribution Theory and Fourier Transforms*. Singapore, World Scientific Publishing Company, 2003.

Rana Jafari received the B.A. degree from Harvard University in 1977 and the Ph.D. degree from Stanford University in 1983. He is currently pursuing the Ph.D. degree in physics with the Georgia Institute of Technology.

Rick Trebino was born in Boston, MA, USA, in January 1954. He received the B.A. degree from Harvard University in 1977 and the Ph.D. degree from Stanford University in 1983.

In 1986, he moved to Sandia National Laboratories, Livermore, CA, USA, where he studied higher-order wave-mixing, nonlinear-optical perturbation theory using Feynman diagrams, and ultrashort-laser-pulse techniques with application to chemical dynamics measurements and combustion diagnostics. There he developed frequency-resolved optical gating (FROG), the first technique for the measurement of the intensity and phase of arbitrary ultrashort laser pulses. In 1998, he became the Georgia Research Alliance-Eminent Scholar Chair of ultrafast optical physics with the Georgia Institute of Technology, Atlanta, GA, USA, where he currently researches ultrafast optics and applications. His dissertation research involved the development of a technique for the measurement of ultrafast events in the frequency domain using long-pulse lasers by creating moving gratings. He continued this research during a three-year term as a Physical Sciences Research Associate at Stanford.

Prof. Trebino is also a fellow of the Optical Society of America, the American Physical Society, the American Association for the Advancement of Science, and the Society of Photo-Instrumentation Engineers. He was a recipient of the SPIE's Yzuel Award for his pioneering contributions to optics education. He has received numerous prizes, including the SPIE's Edgerton Prize and an R&D 100 Award. He was an IEEE Lasers and Electro-Optics Society Distinguished Lecturer.

Authorized licensed use limited to: Georgia Institute of Technology. Downloaded on December 09,2020 at 18:47:12 UTC from IEEE Xplore. Restrictions apply.